Long-Lived Photogenerated States of α-Oligothiophene−Acridinium Dyads Have Triplet Character

Jingqiu Hu,[†] Bing Xia,[†] Duoduo Bao,[‡] Amy Ferreira,[‡] Jiandi Wan,[†,‡] Guilford Jones II,*[,†] and Valentine I. Vullev*[,‡]

Department of Chemistry and Photonics Center, Boston University, Boston, Massachusetts 02215, and Department of Bioengineering, University of California, Riverside, California 925521

Received: December 11, 2008; Revised Manuscript Received: January 25, 2009

Photoinduced processes, leading to charge-transfer states with extended lifetimes, are of key importance for solar-energy-conversion applications. Utilizing external heavy-atom effect allowed us to photogenerate long-lived transients of electron donor−acceptor dyads. For an electron acceptor and a principal chromophore of the dyads, we selected *N*-methylacridinium, and for electron donors thiophene, bithiophene, and terthiophene were selected. While the photoinduced charge transfer, mediated by the investigated dyads, occurred in the picosecond time domain, the lifetime of the transients extended to the microsecond time domain. We ascribed the relatively long lifetimes to the triplet character of the observed transients. An increase in the size of the donor lowered the energy of the charge-transfer states of the dyads. When the energy level of the acridinium triplet lies below the energy level of the charge-transfer state, the locally excited triplet accounted for the long-lived transient. For the conjugates with charge-transfer states lying below all other excited states, the long-lived transients were, indeed, the charge-transfer species.

Introduction

This publication describes electron donor−acceptor dyads that efficiently mediate photoinduced charge transfer occurring in the picosecond time domain. In the presence of a brominated solvent, we observed transients in the microsecond time domain. These long-lived transients were either locally excited triplets or charge-transfer species, depending on the relative energies of the triplet and the charge-transfer states of the different dyads.

Donor−acceptor systems, which efficiently mediate photoinduced charge transfer and impede the back charge transfer processes, are of enormous importance for solar-energy-conversion applications.[1−4] Utilization of triplet formation,[2,5−8] media viscosity,[9−11] solvent polarity,[12] and local electric fields[13−18] allows for photogeneration of long-lived charge-transfer species.

Others and we have extensively studied dyads and triads containing acridinium as an electron acceptor and a principal chromophore.[9,19−28] Such donor−acridinium dyads mediate efficient photoinduced charge transfer, occurring within a few picoseconds;[25−27] i.e., the photoexcitation of the positively charged acridinium allows it to extract an electron from the covalently bonded donor, producing neutral acridinium radical and a radical cation of the donor. The back charge transfer (in which the positive charge shifts back to the acridinium, bringing the dyad back to its ground state) can be 1−3 orders of magnitude slower than the initial photoinduced electron transfer.[25−27]

For certain acridinium dyads, especially when trapped in low-temperature solid matrices, the fast photoinduced charge shift (CSh) leads to long-lived transients that were ascribed to charge-transfer species.[19,29,30] As Verhoeven et al. showed, however, such assignments carry ambiguity due to the overlap and similarities between the transient absorption spectra of the acridinium triplet and the acridinium reduced radical transients.[20,31−33] We, indeed, have observed long-lived CSh species generated from photoexcitation of donor−acridinium dyads in solid glass matrix at room temperature.[9] Singlet CSh states of such dyads can certainly manifest lifetimes in the nanosecond time domain.[9,25−27] The transients detected in the microsecond time domain, however, are ascribed to CSh states with a triplet character.[9] In accordance with our previous findings, solid matrices and external heavy-atom effect propend triplet formation from the twisted excited states of donor−acridinium dyads.[24]

The origin of microsecond transients from picosecond photoinduced charge-transfer processes can be seemingly ascribed as a corollary of pushing the back electron transfer into the inverted Marcus region.[34−38] A great degree of caution is required for applying the transition-state Marcus theory to trends of adiabatic (i.e., strongly coupled) donor−acceptor systems. Therefore, such analysis should be taken at its qualitative (rather than quantitative) value and be based on a good understanding of the properties of the system.

Photogeneration of long-lived charge-transfer transients is of enormous importance for basic science and applied engineering.[1,3] Fluorescence and pump−probe transient-absorption studies allowed us to observe donor−acridinium charge-shift species that live for as long as nanoseconds and exhibit CSh fluorescence.[9,25−27] Nanosecond flash photolysis characterization of some of the same systems, however, revealed charge-shift transients with lifetimes in the microsecond time domain that did not exhibit CSh fluorescence.[9] A plausible explanation for the origin of such long-lived nonfluorescent CSh species is a change in the multiplicity of the photoexcited systems. To examine the nature of the long-lived photogenerted transients in similar donor−acceptor conjugates, we prepared a series of donor−acridinium dyads with a range of CSh energies, higher or lower than the energy of the lowest triplet locally excited state of the acridinium.

Thiophene polymers and oligomers have received substantial attention due to their unusual electronic and optical properties

* Corresponding authors, giljones@bu.edu and vullev@ucr.edu.
[†] Boston University.
[‡] University of California, Riverside.

10.1021/jp810909v CCC: $40.75
Published on Web 03/06/2009

SCHEME 1: Structural Formula of the Studied Acridinium Conjugates

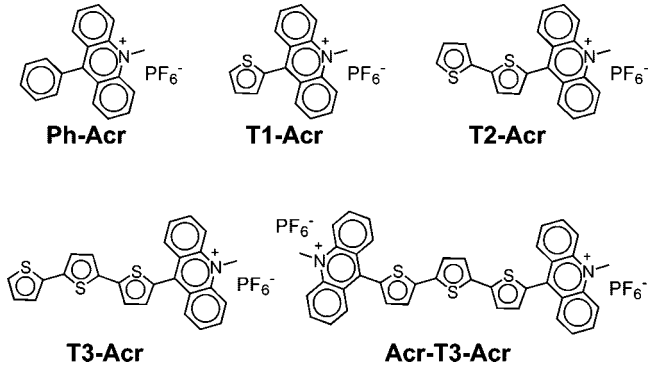

for device applications (e.g., photovoltaic cells and light-emitting diodes).[39−48] For instance, oligothiophenes modified with electron-donating or electron-withdrawing groups, are superior hole-transport or electron-transport materials, respectively.[47] Among the polymer photovoltaic devices, solar cells based on polythiophenes manifest some of the highest power conversion efficiencies.[49−51] A detailed understanding of charge transfer between thiophene oligomers and electron acceptors is essential for optimizing such materials.[12,52−61]

The electronic properties of α-oligothiophenes (T*n*) strongly depend on their sizes.[62−66] This dependence is especially pronounced for the shorter oligomers; i.e., conjugates composed of about six thiophene units or less, i.e., T*n* with $n \leq 6$.[62] For α-oligothiophenes, an increase in the oligomer length (1) decreases the energies of their lowest singlet and triplet excited states[62,67,68] and (2) lowers their oxidation potentials, making them better electron donors.[66,69,70]

We utilized α-oligothiophenes with different lengths as electron donors in dyads containing acridinium as an acceptor (Scheme 1). Changing the length of the donor from one to three units, allowed us to move the energy level of the CSh states of the dyads from above to below the lowest triplet state of the acridinium. For increasing the efficiencies of the intersystem-crossing processes, we utilized external heavy-atom effect; i.e., we used a mixture of 1-bromobutane and acetonitrile as media for the charge-transfer studies in the microsecond time domain. We observed long-lived charge-transfer transients for the dyads with CSh energies lower than their triplet energies. Because transient-absorption spectroscopy allowed us to observe directly the formation of CSh species from locally excited triplet transients, we could conclude that it is the triplet manifolds that affords the microsecond lifetimes of the charge-transfer species in the donor−acridinium dyads.

Results and Discussion

General Considerations. All donor−acceptor dyads contained *N*-methylacridinium (Acr) as an electron acceptor and a principal chromophore (Scheme 1). For electron donors, we chose thiophene (T1), bithiophene (T2), and terthiophene (T3). In addition to the four dyads, bisacridinium terthiophene, Acr-T3-Acr, allowed for comparisons of the donor−acceptor with acceptor−donor−acceptor conjugates.

An increase in the length of the oligothiophenes decreases the energy levels of their lowest singlet excited states, $S_1^{(Tn)}$, from 4.9 to 3.2 eV for size increase from thiophene, T1, to terthiophene, T3 (Scheme 2).[62] For longer oligomers, the levels of the singlet states are even lower: e.g., $S_1^{(T4)} = 2.9$ eV, $S_1^{(T5)} = 2.7$ eV, and $S_1^{(T6)} = 2.6$ eV for quaterthiophene, pentathiophene, and hexathiophene, respectively.[62]Because the lowest singlet excited state of the acridinium, $S_1^{(Acr)}$, lies about 2.7 eV above its ground state (Scheme 2),[20] we limited this study to conjugates that do not contain oligothiophenes longer than terthiophene. For all conjugates discussed in this study, the charge-shift states lie below the singlet locally excited states of acridinium, $S_1^{(Acr)}$, assuring sufficient driving force for photoinduced charge transfer, i.e., for charge shift from $S_1^{(Acr)}$ (Scheme 2).

SCHEME 2: Energy Diagram of the α-Oligothiophene (T*n*) Acridinium (Acr+) Dyads

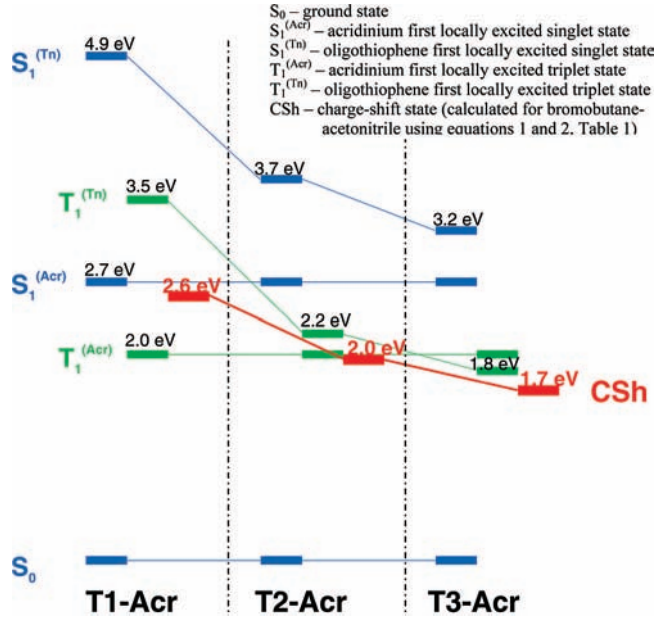

The Rehm−Weller equation allowed us to estimate the driving forces, $\Delta G^{(0)}_{CSh}$, for the photoinduced charge-shift processes[2,71,72]

$$\Delta G^{(0)}_{CSh} = F(E^{(0)}_{Tn^{+\bullet}/Tn} - E^{(0)}_{Acr^{+}/Acr^{\bullet}}) - \mathcal{E}_{00} + \Delta G_S + W \quad (1)$$

where F is the Faraday constant, which is unity (i.e., 1e) if the energy is in electonvolts, $E^{(0)}_{Tn^{+\bullet}/Tn}$ is the standard electrode potential for oxidation of the donor that for T1, T2, and T3 in acetonitrile electrolyte solution are 2.0, 1.4, and 1.1 V vs SCE, respectively,[69,70] $E^{(0)}_{Acr^{+}/Acr^{\bullet}}$ is the standard electrode potential for reduction of acridinium that for acetonitrile electrolyte solution is −0.55 V vs SCE,[73,74] $\mathcal{E}_{00}$ is the zero-to-zero energy for the transition between the ground state and the lowest singlet locally excited state, which is 2.7 eV, and W is the Coulomb correction term, which for charge-shift processes is always zero. For charge shift, initiated from a triplet locally excited state, $\mathcal{E}_{00}$ represents the triplet energy of the acridinium or of the oligothiophenes.

The Born correction term, ΔG_S, in eq 1 accounts for the differences between the ion-solvation energies for the media used for the electrochemical and spectroscopic measurements[72,75,76]

$$\Delta G_S = \frac{e^2}{8\pi\varepsilon_0}\left(\frac{1}{r_{Tn}}\left(\frac{1}{\varepsilon} - \frac{1}{\varepsilon_{Tn}}\right) - \frac{1}{r_{Acr^{+}}}\left(\frac{1}{\varepsilon} - \frac{1}{\varepsilon_{Acr^{+}}}\right)\right) \quad (2)$$

where r_{Tn} is the radius of oligothiophene moieties that for T1, T2, and T3 are 2, 3.5, and 5 Å, respectively, $r_{Acr^{+}}$ is the radius

of the acridinium moiety that is 3 Å, ε_{Tn} and ε_{Acr^+} are the dielectric constants of the media, in which the redox potentials for the donor and the acceptor, respectively, were measured, and ε is the dielectric constant of the media, in which the photoinduced charge shift was studied and $\mathcal{C}_{00}$ was measured.

For the charge-transfer studies we chose three different organic solvents: (1) acetonitrile, which is relatively polar (dielectric constant, $\varepsilon = 36.6$), (2) dichloromethane, which is relatively nonpolar ($\varepsilon = 8.93$), and (3) 12.5% (v/v) 1-bromobutane in acetonitrile, which is a solvent media for providing external heavy-atom effect. Triangular-waveform capacitance measurements[77−79] allowed us to determine the dielectric constant of the bromobutane−acetonitrile solvent mixture, $\varepsilon = 31.7 \pm 0.3$ (Figure 1).

Triangular-waveform capacitance measurements[77−79] are a type of fast-scan cyclic voltammetry on a two-electrode cell. When a triangular-waveform potential is applied to a purely resistive load, i.e., a load with zero reactance, the current response will be a triangular wave with the same phase and with amplitude determined from Ohm's law. If the same triangular-waveform potential is applied to a purely capacitive load, however, the current signal will assume a rectangular waveform with amplitude linearly proportional to the capacitance of the load. Strictly speaking, depending on the slew rate of the applied triangular potential, the current signal follows the charging (or discharging) of the capacitor; i.e., at each point of an abrupt change in the direction of the applied potential, the current signal follows an exponential rise or decay, asymptotically approaching steady-state values maintained by the constant increase (or decrease) in the applied voltage. The time constants of these exponential charging (or discharging) steps decrease with an increase in the difference between the slopes before and after the points of changes in the triangular waveforms. Therefore, applying potential with high-frequency triangular waveforms results in current with rectangular waveforms. For our studies, we utilized 100 kHz triangular waveforms (Figure 1a).

We placed a series of organic solvents, with known dielectric constants, between electrodes of a capacitance sample cell and recorded the current responses for various voltage amplitudes and electrode-separation distances. The obtained current signals had waveforms that were superposed in-phase triangular and rectangular waves (Figure 1b). Deconvolution of the current signals allowed us to extract the rectangular components of the waveforms and determine their amplitudes. Linear fits of the amplitude of the rectangular wave components versus the dielectric constants of the tested solvents yielded calibration curves for each set of conditions used (Figure 1c). Imputing the measured amplitudes for the bromobutane−acetonitrile solution into the linear calibration functions allowed us to determine the dielectric constant (Figure 1c).

Equations 1 and 2 allowed us to estimate the driving force of the photoinduced charge shift, $\Delta G^{(0)}_{CSh}$, and the energy of the charge-shift state, $\mathcal{C}_{CSh} = \mathcal{C}_{00} + \Delta G^{(0)}_{CSh}$, for the oligothiophene−acridinium (Tn−Acr) conjugates in the three chosen solvent media (Tables 1 and 2). The negative values of $\Delta G^{(0)}_{CSh}$ for T2−Acr and T3−Acr translate in picosecond time constants for the photoinduced charge shift processes through the covalent bond providing the donor−acceptor coupling.[25−27]

Absorption Properties of the α-Oligothiophene−Acridinium Conjugates. The UV−vis absorption spectra of the acridinium conjugates display a sharp band around 360 nm (molar extinction coefficient, $\varepsilon \sim 19000\ M^{-1}\ cm^{-1}$) that corresponds to the excitation from the ground state to the second singlet locally excited state of the acridinium, $S_2^{(Acr)} \leftarrow S_0$ (Figure 2). The transition to the acridinium lowest singlet locally excited state ($S_1^{(Acr)} \leftarrow S_0$, $\lambda_{max} \sim 420$ nm), however, is not always a discernible feature of the absorption spectra of donor−acridinium dyads. When the acridinium is derivatized with a redox-inert substituent, such as phenyl (e.g., Ph-Acr), the transition to the $S_1^{(Acr)}$ locally excited state is apparent in the absorption spectrum;

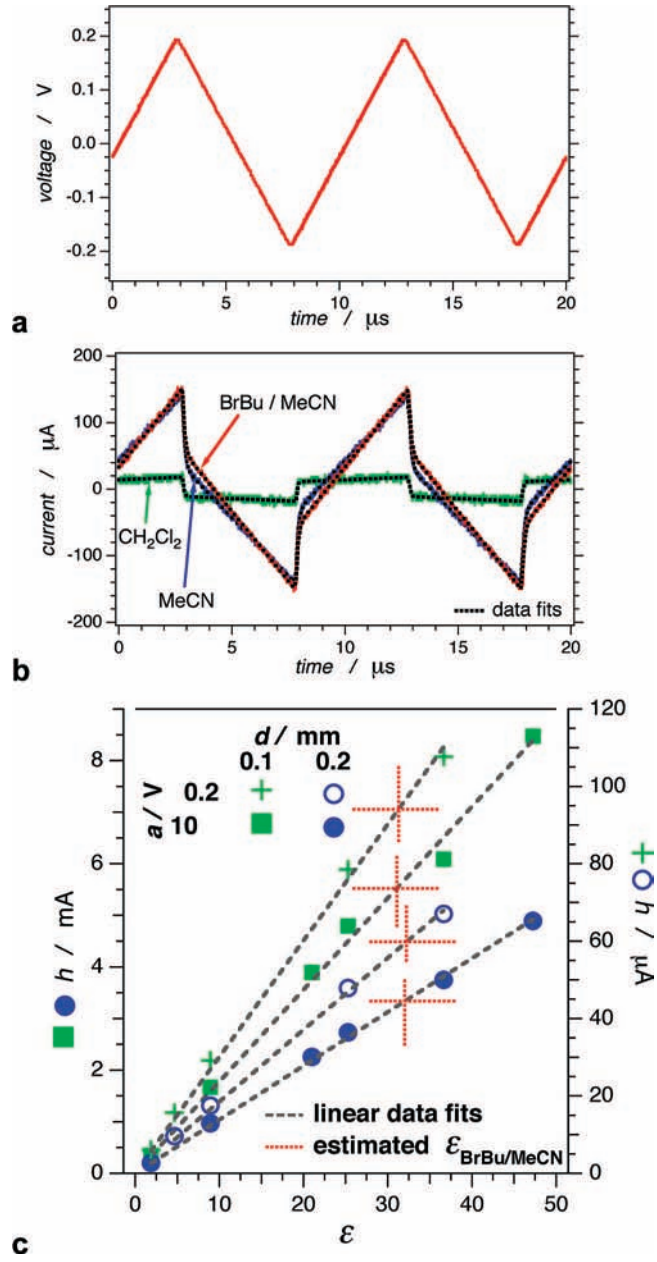

Figure 1. Dielectric measurements of solvents using fast-scan cyclic voltammetry. (a) Triangular waveform of the potential signal (with peak amplitude, $a = 0.2$ V, which is 0.4 V peak-to-peak amplitude) applied to the cell. (b) Current response recorded for three different solvent media with the corresponding data fits representing superimposed triangular and rectangular waveforms ($a = 0.2$ V, and electrode separation, $d = 100$ μm). (c) Graphical estimation of the dielectric constant of 12.5% (v/v) 1-bromobutane (BrBu) in acetonitrile (MeCN). Linear fits of the measured heights of the rectangular waveforms, h, vs the dielectric constants of selected solvents (hexane, chloroform, dichloromethane, acetone, ethanol, acetonitrile, and dimethyl sulfoxide) allowed for callibration for various electrode separations and voltage amplitudes. The unknown dielectric constant, $\varepsilon_{BrBu/MeCN}$, was estimated from the measured height, h, for the bromobutane−acetonitrile mixture and the callibration lines.

TABLE 1: Estimated Photoinduced Charge-Shift Driving Forces, $\Delta G^{(0)}_{CSh}$, and the Corresponding Born Correction Terms, ΔG_S, for the α-Oligothiophene−Acridinium Dyads[a]

		solvent media[b]		
conjugate		MeCN	BrBu/MeCN	CH_2Cl_2
T1−Acr	$\Delta G^{(0)}_{CSh}$[c]	–0.15	–0.14	–0.05
	ΔG_S[d]	0.00	0.01	0.10
T2−Acr	$\Delta G^{(0)}_{CSh}$[c]	–0.75	–0.75	–0.78
	ΔG_S[d]	0.00	0.00	–0.03
T3−Acr	$\Delta G^{(0)}_{CSh}$[c]	–1.1	–1.1	–1.1
	ΔG_S[d]	0.00	0.00	–0.08

[a] The values of $\Delta G^{(0)}_{CSh}$ and ΔG_S are represented in eV. [b] Acetonitrile (MeCN), 12.5% (v/v) 1-bromobutane in acetonitrile (BrBu/MeCN), and dichloromethane (CH_2Cl_2). [c] $\Delta G^{(0)}_{CSh}$ is calculated using eqs 1 and 2. [d] The values of the Born correction term, ΔG_S, are calculated using eq 2. We approximated the dielectric constants of the acetonitrile electrolyte solutions, ε_{Tn} and ε_{Acr^+}, to the dielectric constant of neat acetonitrile, i.e., $\varepsilon_{Tn} = \varepsilon_{Acr^+} = 36.6$, which for this electrochemical solvent media will introduce an error, smaller than about 0.05 eV, in the estimation of $\Delta G^{(0)}_{CSh}$.[72] Nevertheless, the calculated values of $\Delta G^{(0)}_{CSh}$ manifest a trend, induced by the medial polarity, based on the assumption that the size of the acridinium cation, Acr^+, is larger than the size of the thiophene radical cation, $T1^{+\bullet}$, and smaller than the sizes of the bithiophene and terthiophene radical cations, $T2^{+\bullet}$ and $T3^{+\bullet}$. Due to the similar polarity of MeCN and BrBu/MeCN (i.e., $\varepsilon^{-1} \approx \varepsilon_{Tn}{}^{-1} = \varepsilon_{Acr^+}{}^{-1}$, eq 2), the Born correction term is negligible (i.e., smaller than the thermal energy, $k_BT = 0.025$ eV) for the bromobutane−acetonitrile media.

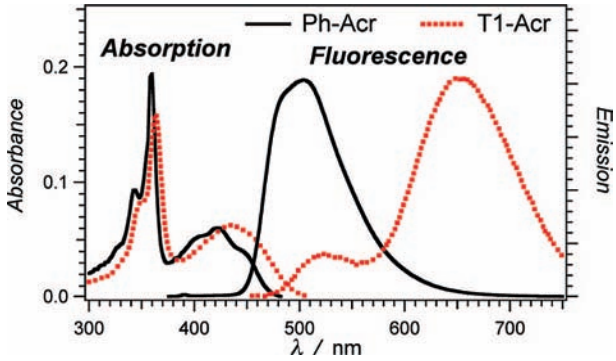

Figure 2. Absorption and normalized fluorescence spectra of Ph-Acr and T1−Acr for acetonitrile. (Conjugate concentration is 10 μM; for the fluorescence spectra, $\lambda_{ex} = 349$ nm.)

i.e., the $S_1{}^{(Acr)} \leftarrow S_0$ transition appears as a broad band, centered at about 420 nm, with discernible vibronic features (Figure 2). The spectrum of T1−Acr shows, however, that when the acridinium is conjugated with an electron-donating moiety, the broad band at 420 nm loses its vibronic features and shifts to the red (Figure 2). This spectral change is a corollary of the appearance of a featureless charge-shift band, $CSh \leftarrow S_0$, that overlaps with the $S_1{}^{(Acr)} \leftarrow S_0$ absorption.

The increase in the length of the oligothiophene moieties improves their electron-donating properties and, hence, lowers the energy of the charge-shift states of the T*n*−Acr dyads, moving the CSh absorption further to the red (Figure 3). The absorption spectra of T3−Acr and Acr−T3−Acr, for which CSh absorption is shifted sufficiently to the red, show a set of weak vibronic features between about 420 and 470 nm that we ascribe to the transition to the S_1 locally excited state of the acridinium (Figure 3).

Increase in the oligothiophene length also lowers the energy of the singlet excited state of the donor, $S_1{}^{(Tn)}$ (Scheme 2). As a result, the spectrum of T2−Acr has a band at about 310 nm that

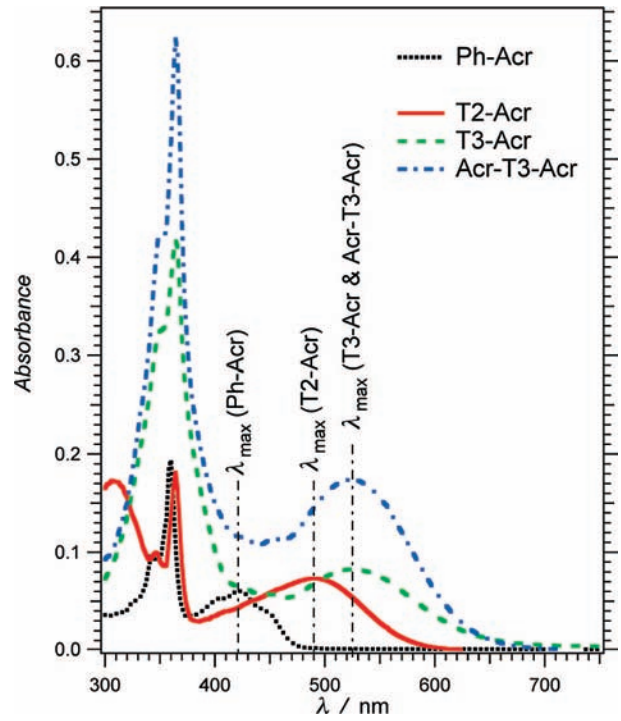

Figure 3. Absorption spectra of Ph-Acr, T2−Acr, T3−Acr, and Acr−T3−Acr for acetonitrile. The vertical dot-dashed lines indicate the peak wavelengths of the red-most absorption bands, λ_{max}. (Conjugate concentration is 10 μM.)

corresponds to the transition to the locally excited state of the bithiophene moiety, $S_1{}^{(T2)} \rightarrow S_0$ (Figure 3). Similarly, the sharp band at about 360 nm in the spectrum of T3−Acr appears broadened and with an increased extinction coefficient. The absorption of the terthiophene, corresponding to the transition to its locally excited state, $S_1{}^{(T3)} \leftarrow S_0$, overlaps with the acridinium absorption, $S_2{}^{(Acr)} \leftarrow S_0$, resulting in the broadened 360 nm band (Figure 3). Comparison between the absorption spectra of Acr−T3−Acr and T3−Acr indicates that an addition of one more electron acceptor to T3−Acr does not cause any spectral shifts. An expected increase in the extinction coefficients at 360 and 450 nm (corresponding to $S_2{}^{(Acr)} \leftarrow S_0$ and $S_1{}^{(Acr)} \leftarrow S_0$, respectively) is obvious for the bis-conjugate, Acr−T3−Acr. A doubling in the intensity of the charge-shift band (~525 nm) resultant from the second acridinium moiety (Figure 3) suggests for an additive effect of the strongly coupled terthiophene with each of the acridiniums attached to the two distal ends of the oligomer.

Although the CSh absorption bands of T3−Acr and its bis-analogue, Acr−T3−Acr, have the same maxima, the addition of Acr to the T3−Acr results in a slight blue shift of the red edge of the absorption spectrum, suggesting for an increase in the charge-shift energy, $\mathcal{E}_{CSh}$ (Figure 3 and Table 2). We ascribe the observed slight increase in $\mathcal{E}_{CSh}$, induced by the addition of another Acr to the dyad, to the destabilization of the charge-shift state of Acr−T3−Acr. Acridinium is a positively charged electron-withdrawing moiety, which does not favor a positive charge localized on the terthiophene, T3, when the conjugate is in its charge-shift state.

According to the calculated values for the charge-shift energy, $\mathcal{E}_{CSh}$ (Table 2), the CSh absorption band should manifest solvatochromism resultant from the difference in the sizes of the donor (oligothiophenes) and the acceptor (acridinium). The Born solvation-energy term, ΔG_S, in the Rehm−Weller equation (eq 1), indicates that a shift of the charge to a smaller (or larger) moiety will destabilize (or stabilize) the CSh state in nonpolar

TABLE 2: Energy of the Charge-Shift States, $\mathcal{E}_{CSh}$, of the α-Oligothiophene−Acridinium Conjugates[a]

	calculated[b]			measured[c]		
conjugate	MeCN	BrBu/MeCN	CH_2Cl_2	MeCN	BrBu/MeCN	CH_2Cl_2
T1-Acr	2.55	2.56	2.65	2.55	2.54	2.49
T2-Acr	1.95	1.95	1.92	2.19	2.16	2.04
T3-Acr	1.65	1.65	1.57	2.07	1.97	1.79
Acr-T3-Acr				2.00	1.99	1.88

[a] Energy is represented in eV for three different solvent media: acetonitrile (MeCN), 12.5% (v/v) 1-bromobutane in acetonitrile (BrBu/MeCN), and dichloromethane (CH_2Cl_2). [b] $\mathcal{E}_{CSh}$ is calculated using eqs 1 and 2: $\mathcal{E}_{CSh} = \Delta G^{(0)}_{CSh} + \mathcal{E}_{00} = F(E^{(0)}_{Tn^{\bullet+}/Tn} - E^{(0)}_{Acr^{\bullet}/Acr^{+}}) + \Delta G_S$. [c] $\mathcal{E}_{CSh}$ is estimated from the absorption spectra of the dyads for different media (Figures 4 and 5): $\mathcal{E}_{CSh} = \hbar c/\lambda_{CSh}$, where $\hbar$ is the Planck's constant (4.14×10^{-15} eV s), c is the speed of light (3.00×10^8 m s^{-1}), and λ_{CSh} is the wavelength of the red edge of the absorption spectra of the dyads, i.e., where the absorbance is 20% of the absorbance at the maximum of the CSh band.

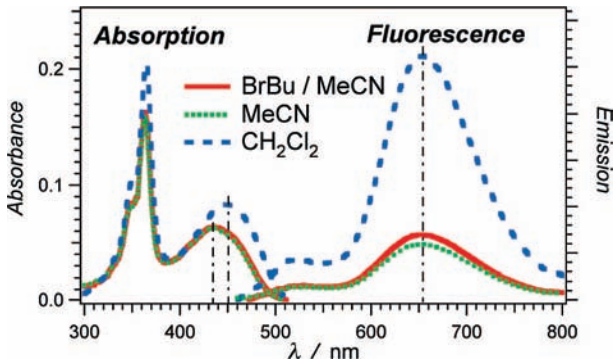

Figure 4. Absorption and fluorescence spectra of T1−Acr for three different solvent media: acetonitrile (MeCN), dichloromethane (CH_2Cl_2), and 12.5% (v/v) 1-bromobutane in acetonitrile (BrBu/MeCN). The dot-dashed lines indicate the peak wavelengths of the red-most absorption and emission bands. (T1−Acr concentration is 10 μM; for the fluorescence spectra, $\lambda_{ex} = 440$ nm.) The calculated fluorescence quantum yields of T1−Acr for MeCN, BrBu/MeCN, and CH_2Cl_2 were 2.0×10^{-3}, 2.2×10^{-3}, and 4.9×10^{-3}, respectively.

solvents (equation 2). For T1−Acr, therefore, it is expected for dichloromethane to cause a blue shift of the CSh absorption in comparison with acetonitrile, while for T3−Acr, the same decrease in the solvent polarity would cause a red shift of the CSh band (Table 2).

Our experimental findings, however, did not agree with some of the trends predicted for the solvatochromism of the CSh absorption of the dyads. For T2−Acr and T3−Acr, indeed, the red spectral shifts with a decrease in the solvent polarity is experimentally observed and predicted through the calculations (Table 2). The Rehm−Weller equation, however, predicts blue shift for T1−Acr with a decrease in the solvent polarity that is contrary to the observed red shift for T1−Acr (Table 2). The recorded spectra show red shift of the CSh bands for all oligothiophene−acridinium conjugates upon transition from acetonitrile to dichloromethane (Figures 4 and 5). Apparently, dichloromethane stabilizes the CSh excited states and/or destabilizes the ground states of all four conjugates.

Certain assumptions in the calculation of ΔG_S (eq 2) provide plausible explanation for this discrepancy between the observed and predicted CSh solvatochromism. For the radius of the acridinium ion, r_{Acr^+}, we considered the size of the whole three-ring polyaromatic system. This approach might be an overestimation of r_{Acr^+} because the positive charge is localized mostly on the nitrogen of the acridinium.[80] As a result, the effective radius of the positive charge on the ground-state acceptor can prove to be smaller that the radii of the positive charge on all three α-oligothiophene moieties while in the charge-shift states. Hence, a decrease in the polarity of the media will decrease the charge-shift energy of all oligothiophene−acridinium conjugates.

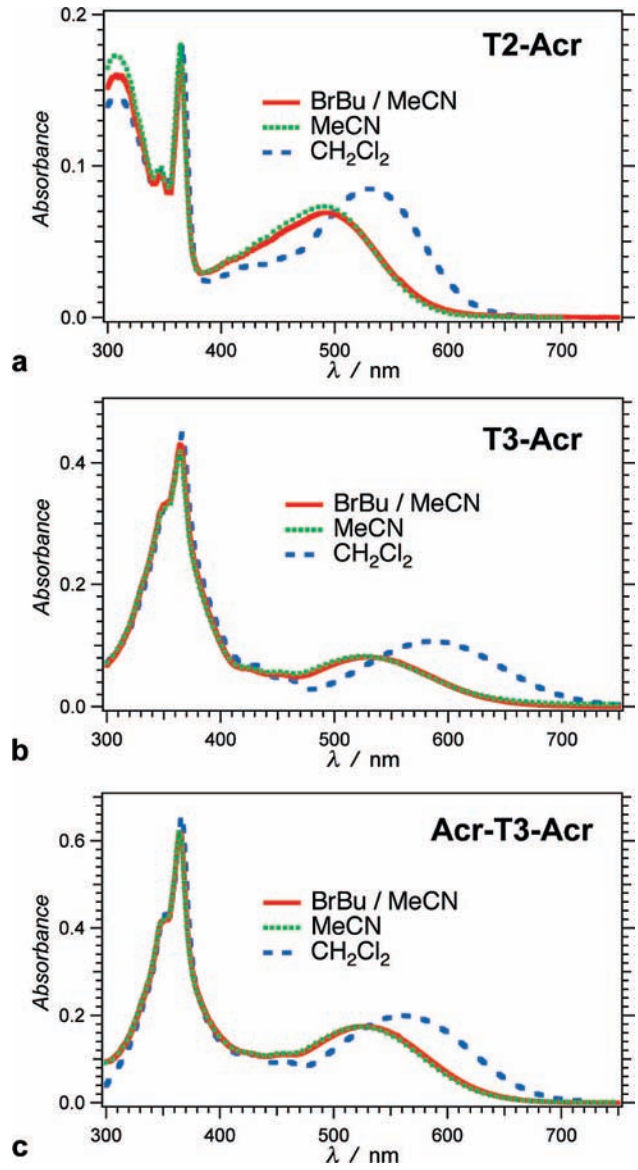

Figure 5. Absorption spectra of (a) T2−Acr, (b) T3−Acr, and (c) Acr−T3−Acr for three different solvent media: acetonitrile (MeCN), dichloromethane (CH_2Cl_2), and 12.5% (v/v) 1-bromobutane in acetonitrile (BrBu/MeCN). (Conjugate concentration is10 μM.)

In our analysis, we did not include the role of the counterion, PF_6^- (Scheme 1). Although it is plausible to assume that for diluted solutions in relatively polar solvents, the role of the counterions is negligible, decrease in the polarity of the media might force the formation of ion pairs and, thus, an increase in the effective local dielectric stabilization for the dyads; i.e., ε

SCHEME 3: Photoinduced Charge Transfer for T1−Acr

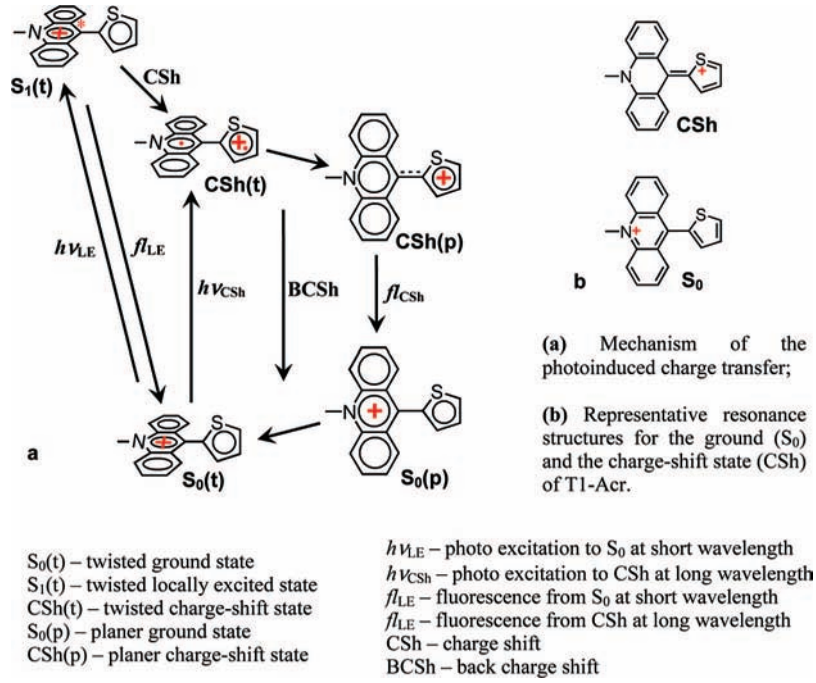

in eq 2 might be underestimated for the solution of these dyad salts in nonpolar solvents.

Emission Properties of T1−Acr. The T1−Acr dyad (9-(2-thiophenyl)-10-methylacridinium hexafluorophosphate) is the simplest of the investigated donor−acceptor conjugates. It has only two covalent single bonds (between non-hydrogen atoms) providing fewer degrees of freedom in comparison with the possible rotamers of T2−Acr, T3−Acr, and Acr−T3−Acr. Furthermore, the charge-shift driving force for T1−Acr is the smallest of the CSh driving forces for the α-oligothiophene−acridinium dyads (Table 2). As a result of the lesser competition arising from possible nonradiative decay pathways, we were able to detect emission from T1−Acr with quantum yields in the range of about 0.002−0.005 (Figure 4) and lifetimes shorter than ∼100 ps (which is the detection limit of the instrument used for this study).

In the absence of an electron donor (e.g., Ph-Acr) the acridinium exhibits a strong fluorescence (Figure 2), with λ_{max} = 503 nm and lifetimes 2.5 and 1.5 ns for acetonitrile and dichloromethane, respectively.[26] The emission spectrum of the T1−Acr, however, manifests two distinct bands, λ_{max} = 526 nm and λ_{max} = 653 nm (Figure 2). We can ascribe the blue-shifted band to fluorescence from the locally excited acridinium state, $S_1^{(Acr)} \rightarrow S_0$. The red-shifted band, which has prevalent intensity in the recorded spectra, corresponds to the fluorescence from the charge-shift state of the dyad, CSh → S_0.[9,25−27]

The intensity of the fluorescence band resultant from the acridinium locally excited state is about 6% of the total emission intensity of T1−Acr. For T1−Acr, therefore, the quantum yields for the fluorescence from the acridinium locally excited state range between about 1×10^{-4} and 3×10^{-4} for acetonitrile and dichloromethane. An assumption that the addition of an electron donor to the acridinium does not change its radiative-decay rate constant, $k_f(S_1^{(Acr)} \rightarrow S_0)$, allows us to estimate the rate constants, k_{CSh}, of the photoinduced charge shift for T1−Acr

$$k_{CSh} = \left(\frac{\Phi_0}{\Phi} - 1\right)\frac{1}{\tau_0} \qquad (3)$$

where Φ_0 and Φ are the fluorescence quantum yields of acridinium in the absence and presence of an electron donor, respectively; and τ_0 is the lifetime of acridinium in the absence of an electron donor. Using the quantum yield and the lifetime of Ph-Acr for Φ_0 and τ_0,[26] we estimated a charge-shift rate constant for T1−Acr in the range of 10^{11} s^{-1}.

The fluorescence spectra of T1−Acr in different solvents reveal that, unlike the CSh absorption, the CSh fluorescence does not shift with the change in the solvent polarity (Figure 4). Furthermore, the red edge of the T1−Acr absorption is more than 50 nm separated from the CSh fluorescence. These findings suggest that the observed CSh absorption and the CSh fluorescence do not involve the same charge-shift state.

For conjugates of acridinium with aromatic groups, the ground-state twisted structures are more stable than their ground-state planar structures. Due to the steric hindrance between the thiophene β_3-hydrogen with the hydrogens at the 1 and 8 positions of the acridinium, the twisted conformation will be prevalent for the ground-state T1−Acr. In fact, semiempirical molecular-orbital calculations for T1−Acr yielded optimized structures with 55° dihedral angle between the planes of the thiophene and of the acridinium ring system.

For the charge-shift state, however, the planar structures become more stable than the twisted structures. The charge-shift states of donor−acridinium conjugates have biradical character. The interaction between the radicals (for singlet CSh states) can produce partial π-conjugation along the single bond connecting the two aromatic systems. Overcoming the steric hindrance with such electronic stabilization can yield a favorable planar conformation for the singlet charge-shift state of T1−Acr.

The photoexcitation of T1−Acr occurs from its ground-state twisted rotamer, generating a twisted CSh state (Scheme 3). This transition corresponds to the CSh absorption band that manifests solvatochromism (Figure 4). Consequent relaxation of the twisted CSh state leads to the more stable planar CSh state, from which the radiative decay to the planar ground state corresponds to the fluorescence band observed at 653 nm (Scheme 3). Because the planar structures allow similar delo-

calization of the positive charge for both the ground and the charge-shift states (Scheme 3b), such a transition between the two planar states should not manifest solvatochromism; i.e., for the planar rotamers, the effective radii of the donor and the acceptor will be equal, $r_{Acr^+} \approx r_{Tn}$, making $\Delta G_S \approx 0$ (eq 2).

External Heavy-Atom Effect. In our spectral analysis, we were particularly interested in the modulation of the photophysical properties of the donor−acridinium conjugates, induced by chemically and spectrally inert compounds containing elements with relatively large atomic weights. To introduce external heavy-atom effect, we utilized a solvent mixture containing 12.5% (v/v) 1-bromobutane in acetonitrile.

The absorption spectra of the oligothiophene−acridinium conjugates for acetonitrile and for bromobutane/acetonitrile media appeared almost identical (Figures 4 and 5). The addition of bromobutane to acetonitrile, however, caused about 10% increase in the fluorescence quantum yield of T1−Acr (Figure 4). This observation is consistent with our findings for the neat acetonitrile and dichloromethane; i.e., halogenated nonpolar media caused an increase in the emission quantum yield of T1−Acr (Figure 4).

The observed increase in the emission intensity upon addition of bromobutane to acetonitrile, however, occurred solely for the charge-shift band of the fluorescence spectrum, while dichloromethane caused an increase in the intensity throughout the whole spectrum (Figure 4). This finding suggests that bromobutane partially quenches the emission band at the blue side of the fluorescence spectrum of T1−Acr that corresponds to transitions from the twisted locally excited state. In accordance with our previous findings, the twisted conformation of donor−acridinium dyads appears to provide spin−orbital coupling essential for efficient intersystem crossing.[24] Our current and previous findings suggest that, through a heavy-atom effect, bromobutane induces the formation of triplets that competes with other decay pathways for the twisted excited state of T1−Acr.

Long-Lived Photogenerated Transients. Nanosecond transient absorption spectroscopy[81] allowed us to observe transient species resultant from photoexcitation of α-oligothiophene−acridinium conjugates only in the presence of 1-bromobutane. While for neat solvents (i.e., acetonitrile and dichloromethane, in the absence of bromobutane) we did not detect any transients using nanosecond laser flash photolysis, the lifetimes of the transients photogenerated in the presence of bromobutane extended well into the microsecond time domain (Figures 6 and 7).

Photoexcitation of T1−Acr in the presence of bromobutane produced transient spectra that are representative of the locally excited triplet of the acridinium moiety, $^3Acr^{+}$* (Figure 6a). The spectrum of $^3Acr^{+}$* has broad features that spread from the UV to the midrange of the visible region and manifest dips at wavelengths corresponding to the steady-state absorption of the acridinium conjugate due to depletion of the ground state of the dyad (Figure 6a).[20,32]

When the triplet state lies bellow the charge-transfer state, the locally excited triplet species can be formed upon back electron transfer.[8] The triplet acridinium is, indeed, the lowest excited state of T1−Acr (Scheme 2). In accordance with our fluorescence measurements, however, the heavy-atom effect induces triplet formation from the twisted locally excited state of the dyad, i.e., T1−^{1}Acr* → T1−^{3}Acr*. This evidence, therefore, suggests that the formation of the observed long-lived transient for T1−Acr does not involve charge-shift pathways.

The transient absorption spectra of the bithiophene conjugate, T2−Acr, appear as a composition of relatively weak features

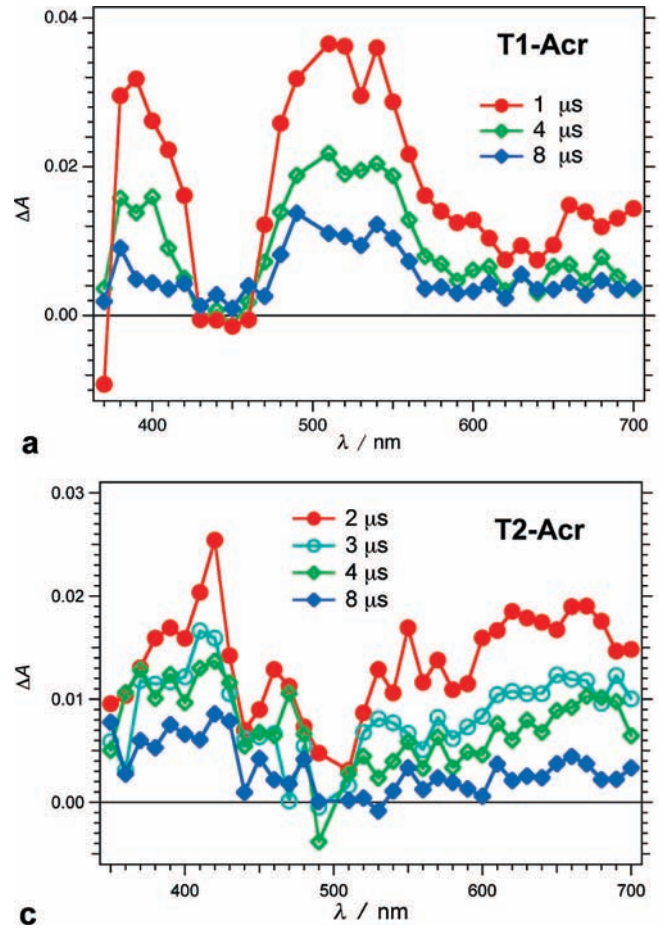

Figure 6. Time-resolved absorption spectroscopy of (a, b) T1−Acr and (c, d) T2−Acr for 12.5% (v/v) 1-bromobutane in acetonitrile. (a, c) Transient absorption spectra. (b, d) Transient decays at different wavelengths with the corresponding monoexponential data fits (solid black lines) and residuals. (λ_{ex} = 355 nm, half-height pulse width = 8 ns.)

of the transients of the lowest triplet locally excited states and of the charge-transfer species (Figure 6c).[20,32,82,83] The transient of the acridinium radical, Acr$^\bullet$, absorbs between about 500 and 600 nm, overlapping with the acridnium triplet, $^3Acr^{+}$*.[20,32] The bleach of the charge-shift ground-state absorption band of T2−Acr (Figure 3) cancels the broad spectral features of the acridinium transients, leaving a dip at around 480−500 nm in the transient spectra of T2−Acr. As a result, the 450 nm band (at early times) is ascribed to $^3Acr^{+}$*, and the 520−600 nm band is ascribed to Acr$^\bullet$ and $^3Acr^{+}$* (Figure 6c). The band with a maximum at ∼420 nm corresponds to the absorption of the bithiophene radical-cation transient, T2$^{+\bullet}$.[82,83] Concurrently, the broad shoulder at 490 nm can be ascribed to traces of bithiophene triplets, ^{3}T2*.[82] We ascribe the broad band between 600 and 700 nm also to a bithiophene transient; it is a transient spectral feature of T2−Acr when placed in viscous media, such as solid matrix or polymer solutions, and is not observed for the other acridinium conjugates.

Our observations suggest that the long-lived T2−Acr transients are a result of triplet species (i.e., ^{3}(T2$^{+\bullet}$−Acr$^\bullet$), T2−^{3}Acr^{+}*, and ^{3}T2*−Acr$^+$), which could be a corollary of the isoenergetic character of the charge shift and the lowest triplet excited states of T2−Acr (Scheme 2). The reported values for the acridinium triplet energy range between about 1.8 and 2.3 eV, depending on the substituents at positions 9 and 10 of the polycyclic aromatic system.[84] The reported triplet energy

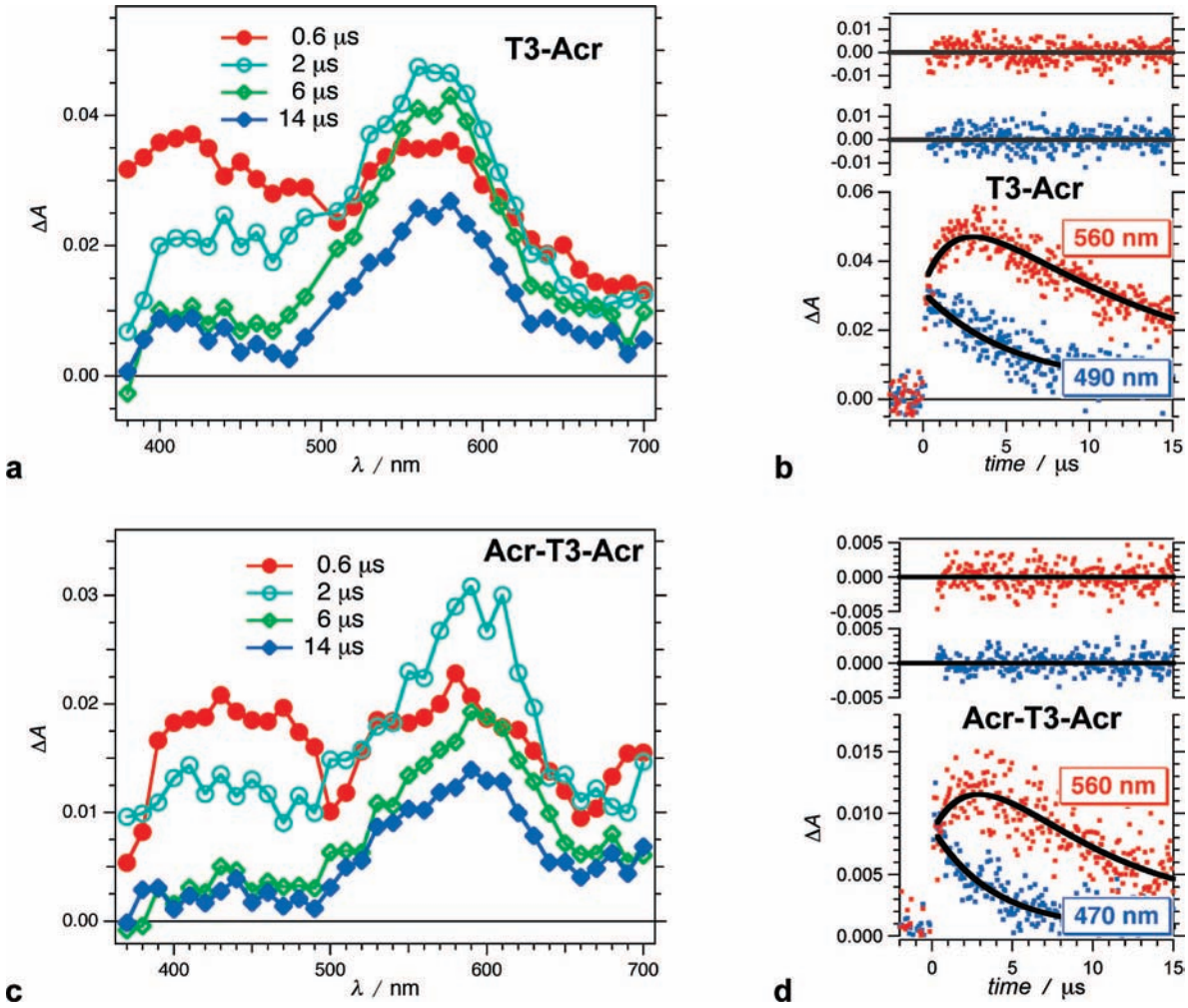

Figure 7. Time-resolved absorption spectroscopy of (a, b) T3−Acr and (c, d) Acr−T3−Acr for 12.5% (v/v) 1-bromobutane in acetonitrile. (a, c) Transient absorption spectra. (b, d) Transient decays at different wavelengths with the corresponding monoexponential and biexponential (i.e., rise-decay at 560 nm) data fits (solid black lines) and residuals. (λ_{ex} = 355 nm, half-height pulse width = 8 ns.)

of bithiophene is about 2.2 eV.[62,63] The charge-shift energy, $\mathcal{E}_{CSh}$, of T2−Acr for bromobutane−acetonitrile solution, estimated from the ground-state absorption spectra is about 2.2 eV, and from eqs 1 and 2 is about 2.0 eV (Table 2).

The value of the triplet energies for T*n*−Acr dyads should be considered with caution because they are based on data for the isolated oligothiophenes and not for the conjugates.[62,63] As demonstrated for acridinium, the strong electronic coupling with substituents shifts its triplet energy.[84] Therefore, the triplet energy of the dyad, ^{3}T2*−Acr$^+$, may be slightly different from the triplet energy of the bithiophene itself, ^{3}T2*.

The values of the T*n*−Acr charge-shift energies estimated from its absorption spectrum (Table 2) correspond to its singlet charge-shift state, ^{1}(T2$^{+\bullet}$−Acr$^\bullet$). The strong electronic coupling between the oligothiophenes and the acridinium will result in triplet charge-shift energies, ^{3}(T2$^{+\bullet}$−Acr$^\bullet$), that are smaller than the singlet energies determined from the steady-state ground-state absorption.

The transient spectra of T2−Acr for bromobutane−acetonitrile media show evidence for the presence of the three triplet states, ^{3}(T2$^{+\bullet}$−Acr$^\bullet$), T2−^{3}Acr$^+$*, and ^{3}T2*−Acr$^+$, decaying with similar rates. Such coexistence of these long-lived phootgenerated species can be ascribed to two extreme cases. (1) The energies of three triplet states of T2−Acr are extremely close to one another, i.e., within less than the thermal energy, k_BT, resulting in establishing of equilibrium quickly within the time of the measurement. (2) Each of the three triplet states of T2−Acr are generated through different pathways, and the kinetics of conversion from one to another is considerably slower than the time of measurements, allowing them to decay independently to the ground state. The simultaneous decays of the T2−Acr transients, along with the preceding evidence for strong coupling, strongly suggest that the latter case does not represent a plausible scenario for the long-lived photogenerates species. Therefore, we ascribe the observed transients to ^{3}(T2$^{+\bullet}$−Acr$^\bullet$), T2−^{3}Acr$^+$*, and ^{3}T2*−Acr$^+$ in thermal equilibrium, decaying simultaneously to ground state.

In the presence of bromobutane, the transient spectra of the terthiophene conjugates, T3-Acr and Acr-T3-Acr, manifest patterns and microsecond dynamics that differ from the observed transient behavior for the dyads of the shorter oligomers (Figure 7). The early appearance of a broad absorption band centered around 460 nm, which we ascribe to the terthiophene triplet,[82,85] indicates that upon photoexcitation and intersystem crossing the systems relax to their lowest triplet locally excited states, ^{3}T3*−Acr and Acr−^{3}T3*−Acr (Scheme 2).

A rise of an absorption band centered at about 560 nm, with a shoulder at its blue edge, accompanies the decay of the terthiophene triplet transient (Figure 7). We ascribe the 560 nm transient absorption to the terthiophene radical cation[82,83,85] and the shoulder at about 530 nm to the acridinium radical.[20,32] This observation indicates that the triplet locally excited state of the

terthiophene moiety initiates electron transfer to the acridinium, producing triplet charge-shift states of the conjugates.

The microsecond charge-shift kinetics for the observed triplet manifold process, i.e., ^{3}T3*−Acr$^+$ → ^{3}(T3$^{+\bullet}$−Acr$^\bullet$), is considerably slower than the kinetics of singlet-manifold charge shifts with just slightly larger driving force; e.g., for T1−^{1}Acr$^+$* → ^{1}(T1$^{+\bullet}$−Acr$^\bullet$), $\Delta G^{(0)}_{CSh} = -0.15$ eV (Tables 1 and 2) and $k_{CSh} \approx 10^{11}$ s^{-1} (eq 3). The difference in the driving forces between the singlet and triplet charge-shift processes (i.e., $\Delta G^{(0)}_{CSh}$ for ^{3}T3*−Acr$^+$ → ^{3}(T3$^{+\bullet}$−Acr$^\bullet$) is between −0.05 and −0.1 eV, as estimated from triplet energy values for ^{3}T3*), however, cannot account for 5 orders of magnitude difference in the observed charge-shift rates.

The above comparison between charge-shift processes mediated by thiophene and terthiophene conjugates, i.e., T1−Acr vs T3−Acr and Acr−T3−Acr, is not truly plausible. While the thiophene donor is a single-ring system, the three rings of the terthiophene are connected with single bonds (Scheme 1) that give T3 additional rotational degrees of freedom. Torsion-angle conformational gating is known to modulate and even impede charge-transfer processes.[86−88] Furthermore, while the singlet manifold CSh process was initiated from acridinium locally excited state, T1−^{1}Acr$^+$*, the triple process was initiated from the donor locally excited state, ^{3}T3*−Acr$^+$.

For fair comparison, we can make a parallel between the singlet and triplet charge-shift processes observed for the terthiophene conjugates, e.g., T3−^{1}Acr$^+$* → ^{1}(T3$^{+\bullet}$−Acr$^\bullet$) vs ^{3}T3*−Acr$^+$ → ^{3}(T3$^{+\bullet}$−Acr$^\bullet$). The driving force for the singlet process, $\Delta G^{(0)}_{CSh} = -1.1$ eV (Tables 1 and 2), exceeds with an order of magnitude the driving force for the triplet process. Such 1 eV difference in the driving forces can result in more than 5 orders of magnitude difference in the charge-shift rate constants (assuming the semiclassical relationship between k_{CSh} and $\Delta G^{(0)}_{CSh}$; i.e., $k_{CSh} \propto (\Delta G^{(0)}_{CSh} + \lambda)^2/4\lambda k_B T$, where λ is the reorganization energy of the CSh system).[89] Therefore, while the fluorescence quenching dynamics of acridnium suggests a charge-shift occurring in the picosecond time domain, the charge shift initiated from the locally excited triplet occurs from the microsecond time domain. Additional modulation in this difference between the triplet and singlet processes is expected from the different properties of the acridinium, T3−^{1}Acr$^+$*, and terthiophene, ^{3}T3*−Acr$^+$, locally excited state, initiating the charge shift.

It should be emphasized that the charge-shift transient band, located around 560 nm with a 530 nm shoulder, is apparent in the spectra recorded even at the earliest times (Figure 7, parts a and c). Therefore, the locally excited triplet of the terthiophene moieties is not the only source for the observed charge-shift states. Nevertheless, the relatively long lifetimes of the charge-shift states, T3$^{+\bullet}$−Acr$^\bullet$ and Acr−T3$^{+\bullet}$−Acr$^\bullet$, can be attributed to their triplet character.

Conclusions

External heavy-atom effect on α-oligothiophene−acridinium conjugates allows for the photogeneration of long-lived locally excited and charge-transfer states. The microsecond lifetimes of the observed transients are a corollary of their triplet character rather than of the large driving forces for the back charge transfer that may push its kinetics in the inverted Marcus region. We believe that our findings may elucidate the reasons for unusually long lifetimes of charge-transfer states not only of other donor−acridinium but also of other donor−acceptor dyads.

Experimental Section

Materials. 2-Bromothiophene, 2,5-dibromothiophene, thiophene-2-carboxylic acid, bithiophene, *N*-bromosuccinimide, 10-methylacridone, *N*-butyllithium (2.5 M in hexane), dichloro[1,3-bis(diphenylphosphino)propane]nickel(II), 1-bromobutane, and magnesium turnings were purchased from Aldrich. The anhydrous ether and tetrahydrofuran (THF) were obtained from VWR and freshly distilled before use. For spectroscopy measurements, acetnitrile and dichloromethane (>99.9%) were obtained from VWR. For dielectric measurements, hexane, chloroform, dichloromethane, acetone, ethanol, acetonitrile, and dimethyl sulfoxide were obtained from Fisher Scientific. 9-Phenyl-10-methylacridinium hexafluorophosphate (Ph-Acr), was prepared according to a procedure that we previously described.[24,25]

Preparation of α-Oligothiophene−Acridinium Conjugates. The general procedure, which we adopted for the synthesis of acridinium-ion derivatives, involves organolithium addition to the carbonyl group of 10-methyl-9-acridone. The protons on the α-position of thiophene are more acidic than those on the β-position.[90] This acidity difference allowed for selective lithiation of the α-positions with *n*-butyllithium at −70 °C, followed by further coupling using 10-methyl-9-acridone. Excess of the *n*-butyllithium (>4 equiv), however, followed by coupling using 2 equiv of 10-methyl-9-acridone, yielded bis-acridinium oligothiophene conjugates.

Adopting published procedures,[91−95] we prepared the oligothiophenes via a series of condensation steps from 2-bromothiophene, 2,5-dibromothiophene, and bithiophene, i.e., condensation of aryl halide with arylmagnesium bromide[95] and homocoupling of arylithium compounds. We used *N*-bromosuccinimide (NBS) as a bromination agent.[92]

Silica gel (40 μm, 230−400 mesh, Baker) was employed as a stationary phase for flash column chromatography.[96−98] For 0.5−2.0 g crude product, we selected a column, typically 2.5 cm (radius) × 32 cm (height), and we packed about $^1/_3$ of the total height. The samples were loaded using a "dry method", which involves dissolving about 1 g of crude product in a solvent with low boiling point, e.g., dichloromethane, and suspending about 1 g of silica gel into the solution. The solvent was evaporated, and the dry mixture of silica gel and crude sample was loaded onto the packed stationary phase of the column. The purity of the collected fractions was monitored by analytical thin layer chromatography (TLC) using silica gel 60 F 254, coated on plastic back plates (0.2 nm thickness). We used dichloromethane/methanol gradient for eluent: the methanol concentration was increased stepwise from about 2% to 10% (v/v). The R_f value for the desired product on silical gel TLC was approximately 0.2−0.3 (typically, in dichloromethane with 4% methanol).

Melting points (mp) were measured on a microscope slide using a Fischer-Johns melting point apparatus. The high-resolution mass spectra (HRMS) were collected with a Finnegan MAT-90 spectrometer. NMR spectra were recorded on a Varian XL-400 spectrometer (93.94 kG magnet; 400 MHz for ^{1}H, 300 MHz for ^{13}C). The proton, ^{1}H, and the carbon-13, ^{13}C, resonances of the solvents were used for internal reference: for acetone-d_6, ^{1}H and ^{13}C appear at 2.05 and 29.9 ppm, respectively, and for DMSO-d_6, ^{1}H and ^{13}C appear at 2.49 and 39.5 ppm, respectively.

The negatively charged counterions determine the solubility of the acridinium salts. Bulky anions (soft bases), such as hexafluorophosphate (PF_6), usually afford relatively high solubility of acridinium in organic solvents (e.g., CH_3CN, CH_2Cl_2, and hexanes). The halide salts of the acridinium, such as

chloride, bromide, and iodide, show good solubility in aqueous solution and poor solubility in organic solvents. The organic procedures afforded acridnium chloride derivatives. We conducted counterion exchange with PF_6 in order to obtain acridinium derivatives soluble in organic media.

For the moisture-sensitive reaction steps, involving Grignard reagent or *n*-butyllithium, all glassware was baked in the oven at 120 °C for at least 12 h, cooled in a desiccator, and purged with argon prior to use. During the reactions, the vessels were tightly sealed and connected with argon-filled balloons to keep dry inert environment at slightly elevated pressure.

All compounds were purified using column chromatography and recrystallization. For characterization, we employed ^{1}H and ^{13}C NMR and high-resolution mass spectrometry (HRMS). The N-methylated pyridinium carbon displays a key chemical shift around 39.5 ppm (for acetone-d_6 solutions). The other assignments of ^{13}C chemical shift were based on previously reported NMR data for analogous acridinium derivatives.

9-(2-Thiophenyl)-10-methylacridinium Hexafluorophosphate (T1−Acr). Thiophene (0.6 g, 7.1 mmol) and a magnetic spinner were placed in a 500 mL three-neck flask equipped with dropping funnel. The vessel was tightly sealed and connected with an argon-filled balloon. Upon purging with sufficient volume of argon, we injected 50 mL of anhydrous THF into the flask. The mixture was stirred and cooled on a dry ice/acetone bath for 30 min, and 3.5 mL of a 2.5 M solution of *n*-butyllithium (8.8 mmol) in hexane was added dropwise using a 10 mL syringe. The reaction mixture was allowed to warm up to room temperature and stir for 1.5 h. The solution was cooled again over a dry ice/acetone bath for 30 min, and 10-methylacridone (1.0 g, 6.8 mmol) in 150 mL of anhydrous THF was added over 20 min. The reaction mixture was stirred at −78 °C for 30 min and then allowed to warm up to room temperature and stirred for another hour. Dilute hydrochloric acid (20 mL, 1 M) was added to the mixture to convert the metaloorganic compounds to benign salts. The solvents were evaporated under vacuum using a rotary evaporator. The residue was treated with potassium hexafluorophosphate saturated aqueous solution and extracted with chloroform. The extract was evaporated and purified by column chromatography over silica gel. The product was recrystallized from ethanol to afford 1.4 g yellow crystals (yield 75%). Mp: 226−227 °C. ^{1}H NMR (400 MHz, acetone-d_6, δ ppm): 8.93 (d, J = 11.5 Hz, H4, 2H), 8.54 (t, J = 9.5, 10.0 Hz, H3, 2H), 8.37 (d, J = 11.0 Hz, H1, 2H), 8.20 (d, J = 6.5 Hz, Hc, 1H), 8.06 (t, J = 10.5, 9.0 Hz, H2, 2H), 7.68 (d, J = 4.5 Hz, Ha, 1H), 7.57 (t, J = 6.5, 4.5 Hz, Hb, 1H), 5.18 (s, N-CH_3, 3H). ^{13}C NMR (300 MHz, acetone-d_6, δ ppm): 156.09, 143.02 (2C), 140.07, 134.31 (2C), 133.10, 132.36 (2C), 131.05 (2C), 129.52, 129.48 (2C), 128.43, 120.07 (2C), 39.95. HRMS (EI, 70 eV): m/z = 276.0858 (M^+), the calculated exact mass for $C_{18}H_{14}NS^+$ is 276.0847.

9-(2-(5,2′-Dithiophenyl))-10-methylacridinium Hexafluorophosphate (T2−Acr). Using bithiophene (1.2 g, 7.2 mmol), instead of thiophene, in a procedure identical to the procedure for synthesis and purification of T1−Acr, afforded 1.5 g of wine-red crystals (yield 62%) of T2−Acr. Mp: 221−222 °C. ^{1}H NMR (400 MHz, acetone-d_6, δ ppm): 8.94 (d, J = 12.0 Hz, H4, 2H), 8.55 (m, J = 9.5, 11.0 Hz, H3, 4H), 8.09 (t, J = 8.5, 10.5 Hz, H1 and H2, 2H), 7.71 (d, J = 4.5 Hz, 1H), 7.63 (dd, J = 4.5, 6.0 Hz, Hc and Hd), 7.53 (d, J = 4.5 Hz, Ha, 1H), 7.21 (m, J = 4.5, 4.5 Hz, Hb, 1H), 5.17 (s, N-CH_3, 3H). ^{13}C NMR (300 MHz, acetone-d_6, δ ppm): 155.70, 143.10, 140.08 (2C), 135.67 (2C), 131.20 (2C), 129.76 (2C), 129.58 (2C), 128.27, 127.87 (2C), 126.77 (2C), 125.95 (2C), 120.11 (2C), 39.99. HRMS (EI, 70 eV): m/z = 358.0720 (M^+), the calculated exact mass for C_{22} H_{16} N S_2^+ is 358.0724.

2,2″:5′,2″-Terthiophene. Magnesium turnings (1.62 g, 65 mmol) and anhydrous ether (50 mL) were placed in a 250 mL argon-purged three-neck flask equipped with a reflux condenser and connected to an argon-filled balloon. The flask was cooled over an ice−water bath for 30 min. The magnesium turnings were activated by adding crystals of iodine (0.25 g) and methyl iodide (0.25 mL). A solution containing 2-bromothiophene (9.24 g, 65 mmol) was added using a syringe over 30 min. The reaction mixture was stirred at room temperature for 3 h. The solution became orange and bubbles appeared at the surface of the magnesium turnings and only a small amount of a dark residue remained on the bottom of the flask.

A solution of 2,5-dibromothiophene (6.5 g, 32 mmol) in 50 mL of anhydrous ether was placed in another three-neck flask purged with argon. Dichloro[1,3-bis(diphenylphosphino) propane]nickel(II) (0.25 g) was added as a catalyst. Using a dry syringe, we transferred the Grignard reagent from its original vessel and slowly injected it into the 2,5-dibromothiophene solution over 40 min at room temperature. The mixture was heated to reflux overnight. The progress of the reaction was monitored using thin layer chromatography (TLC). After we did not observe any further improvement of the yield, we slowly quenched the reaction with 1 M HCl (60 mL). The ether layer was collected and washed with aqueous sodium bicarbonate solution. The extract was purified by column chromatography using petroleum ether as the eluting solvent. The compound was crystallized from ethanol to yield 4.24 g of a light yellow shiny crystal (70%). Mp: 94−95 °C.

9-(2-(5,2′:5′,2″-terthienyl))-10-methylacridinium hexafluorophosphate (T3-Acr). Using terthiophene (1.5 g, 7.2 mmol), instead of thiophene, in a procedure identical to the procedure for synthesis and purification of T1−Acr, afforded 1.1 g of dark red crystals (yield 40%) of T3−Acr. Mp: 233−234 °C. ^{1}H NMR (400 MHz, acetone-d_6, δ ppm): 8.94 (d, J = 11.5 Hz, H_4, 2H), 8.58 (m, J = 12.0, 11.0 Hz, H_1 and H_2, 4H), 8.10 (t, J = 9.5, 10.0 Hz, H_3, 2H), 7.75 (d, J = 4.5 Hz, Hg, 1H), 7.66 (d, J = 5.0 Hz, Hf and 1H), 7.52 (d, J = 6.5 Hz, He, 1H), 7.49 (d, J = 5.0 Hz, Hd, 1H), 7.40 (d, J = 5.5 Hz, Hc, 1H), 7.35 (d, J = 5.0 Hz, Ha, 1H), 7.14 (m, J = 4.5, 4.5 Hz, Hb, 1H), 5.17 (s, N−CH_3, 3H). ^{13}C NMR (300 MHz, acetone-d_6, δ ppm): 154.75, 143.68, 143.05, 140.04 (2C), 139.05, 137.36, 135.85 (2C), 135.03, 131.52, 131.06 (2C), 129.56 (2C), 128.19, 127.64 (2C), 126.89 (2C), 126.06 (2C), 125.74, 120.09 (2C), 39.96. HRMS (EI, 70 eV) m/z = 440.0575, the calculated exact mass for C_{26} H_{18} N S_3^+ is 440.0601.

Bis(10-methylacridinium)terthiophene Dihexafluorophosphate (Acr−T3−Acr). Terthiophene (0.9 g, 3.6 mmol) and a magnetic spinner were placed in a 500 mL three-neck flask equipped with dropping funnel. The vessel was tightly sealed and connected with an argon-filled balloon. Upon purging with sufficient volume of argon, we injected 40 mL of anhydrous THF into the flask. The mixture was stirred and cooled on a dry ice/acetone bath for 30 min, and 6 mL of 2.5 M solution of *n*-butyllithium (15 mmol) in hexane was added dropwise over 20 min using a 10 mL syringe. A brownish yellow precipitate was formed. After the reaction was allowed to proceed at room temperature for 2 h, *N*-methylacridone (1.5 g, 7.2 mmol) in 150 mL of freshly distilled THF was added, using a syringe, over 20 min. The mixture became a clear brown solution. The cooling bath was removed, and the mixture was allowed to warm to room temperature and stirred for 48 h. Some brownish precipitate formed after 24 h. Aqueous hydrochloric acid (1 M,

80 mL) was added to terminate the reaction, and a dark purple precipitate formed. The solvents were removed by rotary evaporation leaving a dark wet solid. To exchange the counteranion with the hexafluorophosphate anion, a saturated aqueous solution (50 mL) and a saturated acetone solution (20 mL) of potassium hexafluorophosphate were added. Removal of the acetone resulted in precipitate, which was collected by filtration to afford 4 g of black powder. TLC revealed that the mixture contained unreacted starting material, 10-methylacridone, which was separated from the product by column chromatography (silical gel, eluted with methanol in dichloromethane: 2% to 10%). About 0.44 g of black powder was collected and recrystallized twice from acetone/ethanol = 1:3 mixture to produce 250 mg of a dark red powder (yield 7.5%) of Acr−T3−Acr. Mp: 270−273 °C. ^{1}H NMR (acetone-d_6, δ ppm): 8.98 (d, J = 11.5 Hz, H4, 4 H), 8.59 (m, J = 11.0, 10.5 Hz, H2 and H3, 8 H), 8.14 (t, J = 10.0, 9.5 Hz, H1, 4 H), 7.84 (d, J = 4.5 Hz, Hc, 2 H), 7.71 (d, J = 4.5 Hz, Hb, 2 H), 7.62 (s, Ha, 2H), 5.19 (s, 6 H), ^{13}C NMR (300 MHz, acetone-d_6, δ ppm): 154.65 (2C), 143.09 (2C), 140.10 (4C), 136.92 (2C), 135.84 (4C), 132.16 (2C), 131.04 (4C), 129.63 (4C), 128.26 (2C), 127.95 (4C), 126.65(4C), 120.14 (4C), 40.02 (2C). HRMS (EI, 70 eV) m/z = 633.1433, the calculated exact mass for $C_{40}H_{29}N_2S_3^+$ is 632.1415.

Absorption and Emission Spectroscopy. UV−visible absorption spectra were recorded using a Beckman model DU-640B spectrophotometer. Steady-state and time-resolved emission measurements were conducted using a PTI (Photon Technology International, Inc.) spectrofluorometer equipped with a GL-3300 nitrogen laser, a GL-302 dye laser, and a GL-303 frequency doubler. The spectroscopy measurements were conducted at room temperature using 1 cm glass cuvettes. Fluorescence quantum yield of the samples (Φ_S) were calculated from the integrated fluorescence intensity of the sample and a reference (F_S and F_R, respectively) with absorbance values of A_S and A_R, respectively, at the excitation wavelengths[99]

$$\Phi_S = \Phi_R\left(\frac{\int F_S(\lambda)\,d\lambda}{\int F_R(\lambda)\,d\lambda}\right)\left(\frac{1-10^{-A_R}}{1-10^{-A_S}}\right)\left(\frac{n_S}{n_R}\right)^2 \qquad (4)$$

The concentrations of the solutions for calculations of emission quantum yields were selected to provide absorbance values for A_S and A_R between 0.1 and 0.2. For a reference, we used a solution of 9-phenyl-10-methylacridinium hexafluorophosphate (Ph-Acr) in acetonitrile (Φ_R = 0.063).[24]

Nanosecond Transient Absorption. Transient absorption spectra and kinetic curves were recorded using a nanosecond laser flash photolysis system equipped with a Quantel YG-581 Nd:YAG laser. Second (532 nm) and third (355 nm) harmonic generators were used as for providing the excitation wavelengths.[81] Small amounts of acridinium stock solutions (usually 5 mM) were added to 4 mL solvents in a long-neck quartz cuvette (1 × 1 cm), sealed with a rubber septum and through a needle, continuously purged with ultrahigh purity argon (Grade 5, purity: 99.999%) before and during the measurements. The concentration of the solution was adjusted to obtain an absorption in the range between 0.50 and 0.75 at the excitation wavelength.

Dielectric Measurements. The dielectric constant of the 1-bromobutane solvent mixtures were determined from triangular waveform (fast scan two-electrode cyclic voltammetry)[77−79] capacitance measurments using a three-terminal cell (12962, Solartron Analytical, U.K.),[100−102] powered by a 30 MHz synthesized wave function generator (DS345, Stanford Research Systems). The applied voltage (Figure 1a) and the resultant signal current (Figure 1b) were recorded using a 500 MHz digital oscilloscope (54616C, Hewlett-Packard) with 1 MΩ and 50 Ω termination for the voltage and the current, respectively. The recorded waves were transferred to a Windows XP workstation via a General Purpose Interface Bus (GPIB) interface (National Instruments).

A micrometer (no. 350-351, Mitutoyo) fixed to the three-terminal cell allowed us to set the electrode separation with micrometer resolution. We used 0.1 MHz triangular form voltage waves with peak amplitudes of 0.2 and 10 V at electrode separation of 0.1 and 0.2 mm. We selected six solvents with known dielectric properties (hexane, ε = 1.89; chloroform, ε = 4.65; dichloromethane, ε = 8.93; acetone, ε = 21.0; ethanol, ε = 25.3; acetonitrile, ε = 36.6; and dimethyl sulfoxide, ε = 47.2) for constructing the calibration lines (the height/amplitude of the rectangular component of the current vs the dielectric constant of the solvent) for the four different conditions (voltage amplitude and electrode separation, Figure 1c). Measurements of 12.5% (v/v) 1-bromobutane in acetonitrile under the same conditions yielded values of amplitudes of the rectangular component of the current that through the calibration lines were converted into values of the dielectric constant of the media (Figure 1c).

Data Analysis. The data for the spectral and the dielectric measurements were analyzed using IgotPro V. Six (Wavematrics, Inc.), installed on MacOS and Windows XP workstations as we previously described.[9,12,77,103,104]

Acknowledgment. Support of this research by the UC Energy Institute and the Department of Energy, Office of Basic Energy Science, Division of Chemistry Sciences. The support for A. Ferreira was provided by the National Science Foundation (EEC 0649096).

References and Notes

(1) Lewis, N. S. *Inorg. Chem.* **2005**, *44*, 6900–6911.
(2) Verhoeven, J. W.; van Ramesdonk, H. J.; Groeneveld, M. M.; Benniston, A. C.; Harriman, A. *ChemPhysChem* **2005**, *6*, 2251–2260.
(3) Kamat, P. V. *J. Phys. Chem. C* **2008**, *112*, 18737–18753.
(4) Guldi, D. M. *Phys. Chem. Chem. Phys.* **2007**, *9*, 1400–1420.
(5) Duncan, T. V.; Ishizuka, T.; Therien, M. J. *J. Am. Chem. Soc.* **2007**, *129*, 9691–9703.
(6) Di Valentin, M.; Bisol, A.; Agostini, G.; Moore, A. L.; Moore, T. A.; Gust, D.; Palacios, R. E.; Gould, S. L.; Carbonera, D. *Mol. Phys.* **2006**, *104*, 1595–1607.
(7) Jones, G., II.; Lu, L. N. *J. Org. Chem.* **1998**, *63*, 8938–8945.
(8) Jones, G., II.; Vullev, V. I. *Org. Lett.* **2002**, *4*, 4001–4004.
(9) Jones, G., II.; Yan, D.; Hu, J.; Wan, J.; Xia, B.; Vullev, V. I. *J. Phys. Chem. B* **2007**, *111*, 6921–6929.
(10) Wolff, H. J.; Buerssner, D.; Steiner, U. E. *Pure Appl. Chem.* **1995**, *67*, 167–174.
(11) Vauthey, E.; Phillips, D. *Chem. Phys.* **1990**, *147*, 421–430.
(12) Wan, J.; Ferreira, A.; Xia, W.; Chow, C. H.; Takechi, K.; Kamat, P. V.; Jones, G.; Vullev, V. I. *J. Photochem. Photobiol., A* **2008**, *197*, 364–374.
(13) Knorr, A.; Galoppini, E.; Fox, M. A. *J. Phys. Org. Chem.* **1997**, *10*, 484–498.
(14) Fox, M. A.; Galoppini, E. *J. Am. Chem. Soc.* **1997**, *119*, 5277–5285.
(15) Galoppini, E.; Fox, M. A. *J. Am. Chem. Soc.* **1996**, *118*, 2299–2300.
(16) Morita, T.; Kimura, S. *J. Am. Chem. Soc.* **2003**, *125*, 8732–8733.
(17) Yasutomi, S.; Morita, T.; Imanishi, Y.; Kimura, S. *Science* **2004**, *304*, 1944–1947.
(18) Shin, Y.-G. K.; Newton, M. D.; Isied, S. S. *J. Am. Chem. Soc.* **2003**, *125*, 3722–3732.
(19) Fukuzumi, S.; Kotani, H.; Ohkubo, K. *Phys. Chem. Chem. Phys.* **2008**, *10*, 5159–5162.

(20) Benniston, A. C.; Harriman, A.; Li, P.; Rostron, J. P.; Van Ramesdonk, H. J.; Groeneveld, M. M.; Zhang, H.; Verhoeven, J. W. *J. Am. Chem. Soc.* **2005**, *127*, 16054–16064.
(21) Lappe, J.; Cave, R. J.; Newton, M. D.; Rostov, I. V. *J. Phys. Chem. B* **2005**, *109*, 6610–6619.
(22) Rust, M.; Lappe, J.; Cave, R. J. *J. Phys. Chem. A* **2002**, *106*, 3930–3940.
(23) Horng, M. L.; Dahl, K.; Jones, G.; Maroncelli, M. *Chem. Phys. Lett.* **1999**, *315*, 363–370.
(24) van Willigen, H.; Jones, G., II.; Farahat, M. S. *J. Phys. Chem.* **1996**, *100*, 3312–3316.
(25) Jones, G., II.; Farahat, M. S.; Greenfield, S. R.; Gosztola, D. J.; Wasielewski, M. R. *Chem. Phys. Lett.* **1994**, *229*, 40–46.
(26) Jones, G., II.; Yan, D.-X.; Greenfield, S. R.; Gosztola, D. J.; Wasielewski, M. R. *J. Phys. Chem. A* **1997**, *101*, 4939–4942.
(27) Jones, G., II.; Yan, D.-X.; Gosztola, D. J.; Greenfield, S. R.; Wasielewski, M. R. *J. Am. Chem. Soc.* **1999**, *121*, 11016–11017.
(28) Pereira Robson, V.; Gehlen Marcelo, H. *J. Phys. Chem. A* **2006**, *110*, 7539–7546.
(29) Fukuzumi, S.; Kotani, H.; Ohkubo, K.; Ogo, S.; Tkachenko, N. V.; Lemmetyinen, H. *J. Am. Chem. Soc.* **2004**, *126*, 1600–1601.
(30) Ohkubo, K.; Kotani, H.; Fukuzumi, S. *Chem. Commun.* **2005**, 4520–4522.
(31) Benniston, A. C.; Harriman, A.; Verhoeven, J. W. *Phys. Chem. Chem. Phys.* **2008**, *10*, 5156–5158.
(32) Verhoeven, J. W.; van Ramesdonk, H. J.; Zhang, H.; Groeneveld, M. M.; Benniston, A. C.; Harriman, A. *Int. J. Photoenergy* **2005**, *7*, 103–108.
(33) Benniston, A. C.; Harriman, A.; Li, P.; Rostron, J. P.; Verhoeven, J. W. *Chem. Commun.* **2005**, 2701–2703.
(34) Marcus, R. A.; Siders, P. *J. Phys. Chem.* **1982**, *86*, 622–630.
(35) Marcus, R. A. *J. Chem. Phys.* **1970**, *52*, 2303–2304.
(36) Marcus, R. A. *J. Chem. Phys.* **1965**, *43*, 2654–2657.
(37) Marcus, R. A. *J. Phys. Chem.* **1989**, *93*, 3078–3086.
(38) Siders, P.; Marcus, R. A. *J. Am. Chem. Soc.* **1981**, *103*, 748–752.
(39) Hotta, S.; Ichino, Y.; Yoshida, Y. Electronic and Optical Properties of Conjugated Molecular Systems in Condensed Phases; Research Signpost: Trivandrum, India, 2003; pp 615−635.
(40) Fichou, D. *J. Mater. Chem.* **2000**, *10*, 571–588.
(41) Murphy, A. R.; Frechet, J. M. J. *Chem. Rev.* **2007**, *107*, 1066–1096.
(42) Locklin, J.; Roberts, M.; Mannsfeld, S.; Bao, Z. *Polym. Rev.* **2006**, *46*, 79–101.
(43) James, D. K.; Tour, J. M. *Top. Curr. Chem.* **2005**, *257*, 33–62.
(44) Perepichka, I. F.; Perepichka, D. F.; Meng, H.; Wudl, F. *Adv. Mater.* **2005**, *17*, 2281–2305.
(45) Barbarella, G. *Electronic and Optical Properties of Conjugated Molecular Systems in Condensed Phases*; Research Signpost: Trivandrum, India, 2003; pp 79−97.
(46) Hotta, S. *Trans. Mater. Res. Soc. Jpn.* **2004**, *29*, 985–990.
(47) Otsubo, T.; Aso, Y.; Takimiya, K. *J. Mater. Chem.* **2002**, *12*, 2565–2575.
(48) Otsubo, T.; Aso, Y.; Takimiya, K. *Pure Appl. Chem.* **2005**, *77*, 2003–2010.
(49) Chaudhary, S.; Lu, H.; Mueller, A. M.; Bardeen, C. J.; Ozkan, M. *Nano Lett.* **2007**, *7*, 1973–1979.
(50) Zhang, F.; Ceder, M.; Inganaes, O. *Adv. Mater.* **2007**, *19*, 1835–1838.
(51) Kim, K.; Liu, J.; Namboothiry, M. A. G.; Carroll, D. L. *Appl. Phys. Lett.* **2007**, *90*, 163511/163511–163511/163513.
(52) Kanato, H.; Takimiya, K.; Otsubo, T.; Aso, Y.; Nakamura, T.; Araki, Y.; Ito, O. *J. Org. Chem.* **2004**, *69*, 7183–7189.
(53) Yassar, A.; Videlot, C.; Jaafari, A. *Sol. Energy Mater. Sol. Cells* **2006**, *90*, 916–922.
(54) Oseki, Y.; Fujitsuka, M.; Cho, D. W.; Sugimoto, A.; Tojo, S.; Majima, T. *J. Phys. Chem. B* **2005**, *109*, 19257–19262.
(55) Cremer, J.; Baeuerle, P. *Eur. J. Org. Chem.* **2005**, *371*, 5–3723.
(56) Raposo, M. M. M.; Fonseca, A. M. C.; Kirsch, G. *Tetrahedron* **2004**, *60*, 4071–4078.
(57) Van Hal, P. A.; Beckers, E. H. A.; Meskers, S. C. J.; Janssen, R. A. J.; Jousselme, B.; Blanchard, P.; Roncali, J. *Chem.—Eur. J.* **2002**, *8*, 5415–5429.
(58) Nishizawa, T.; Tajima, K.; Hashimoto, K. *J. Mater. Chem.* **2007**, *17*, 2440–2445.
(59) Wuerthner, F.; Vollmer, M. S.; Effenberger, F.; Emele, P.; Meyer, D. U.; Port, H.; Wolf, H. C. *J. Am. Chem. Soc.* **1995**, *117*, 8090–8099.
(60) Hirayama, D.; Takimiya, K.; Aso, Y.; Otsubo, T.; Hasobe, T.; Yamada, H.; Imahori, H.; Fukuzumi, S.; Sakata, Y. *J. Am. Chem. Soc.* **2002**, *124*, 532–533.
(61) Knorr, S.; Grupp, A.; Mehring, M.; Grube, G.; Effenberger, F. *J. Chem. Phys.* **1999**, *110*, 3502–3508.
(62) de Melo, J. S.; Silva, L. M.; Arnaut, L. G.; Becker, R. S. *J. Chem. Phys.* **1999**, *111*, 5427–5433.
(63) Jones, D.; Guerra, M.; Favaretto, L.; Modelli, A.; Fabrizio, M.; Distefano, G. *J. Phys. Chem.* **1990**, *94*, 5761–5766.
(64) Garcia, P.; Pernaut, J. M.; Hapiot, P.; Wintgens, V.; Valat, P.; Garnier, F.; Delabouglise, D. *J. Phys. Chem.* **1993**, *97*, 513–516.
(65) Hill, M. G.; Mann, K. R.; Miller, L. L.; Penneau, J. F. *J. Am. Chem. Soc.* **1992**, *114*, 2728–2730.
(66) Hicks, R. G.; Nodwell, M. B. *J. Am. Chem. Soc.* **2000**, *122*, 6746–6753.
(67) Colditz, R.; Grebner, D.; Helbig, M.; Rentsch, S. *Chem. Phys.* **1995**, *201*, 309–320.
(68) Grebner, D.; Helbig, M.; Rentsch, S. *J. Phys. Chem.* **1995**, *99*, 16991–16998.
(69) Meerholz, K.; Heinze, J. *Electrochim. Acta* **1996**, *41*, 1839–1854.
(70) Waltman, R. J.; Bargon, J.; Diaz, A. F. *J. Phys. Chem.* **1983**, *87*, 1459–1463.
(71) Rehm, D.; Weller, A. *Isr. J. Chem.* **1970**, *8*, 259–271.
(72) Bao, D.; Millare, B.; Xia, W.; Steyer, B. G.; Gerasimenko, A. A.; Ferreira, A.; Contreras, A.; Vullev, V. I. *J. Phys. Chem. A* **2009**, *113*, 1259–1267.
(73) Suga, K.; Ohkubo, K.; Fukuzumi, S. *J. Phys. Chem. A* **2005**, *109*, 10168–10175.
(74) Hapiot, P.; Moiroux, J.; Saveant, J. M. *J. Am. Chem. Soc.* **1990**, *112*, 1337–1343.
(75) Born, M. *Z. Phys.* **1920**, *1*, 45–48.
(76) Rashin, A. A.; Honig, B. *Ann. N.Y. Acad. Sci.* **1986**, *482*, 143–144.
(77) Hong, C.; Bao, D.; Thomas, M. S.; Clift, J. M.; Vullev, V. I. *Langmuir* **2008**, *24*, 8439–8442.
(78) Wu, J.; Stark, J. P. W. *Meas. Sci. Technol.* **2005**, *16*, 1234–1240.
(79) Wu, J.; Stark, J. P. W. *Meas. Sci. Technol.* **2006**, *17*, 781–788.
(80) Suzuki, H.; Tanaka, Y. *J. Org. Chem.* **2001**, *66*, 2227–2231.
(81) Vullev, V. I.; Jones, G., II. *J. Appl. Sci.* **2005**, *5*, 517–526.
(82) Hapiot, P.; Lagrost, C.; Aeiyach, S.; Jouini, M.; Lacroix, J. C. *J. Phys. Chem. B* **2002**, *106*, 3622–3628.
(83) Emmi, S. S.; D'Angelantonio, M.; Beggiato, G.; Poggi, G.; Geri, A.; Pietropaolo, D.; Zotti, G. *Radiat. Phys. Chem.* **1999**, *54*, 263–270.
(84) Kikuchi, K.; Sato, C.; Watabe, M.; Ikeda, H.; Takahashi, Y.; Miyashi, T. *J. Am. Chem. Soc.* **1993**, *115*, 5180–5184.
(85) Matsumoto, K.; Fujitsuka, M.; Sato, T.; Onodera, S.; Ito, O. *J. Phys. Chem. B* **2000**, *104*, 11632–11638.
(86) Laine, P. P.; Bedioui, F.; Loiseau, F.; Chiorboli, C.; Campagna, S. *J. Am. Chem. Soc.* **2006**, *128*, 7510–7521.
(87) Davis, W. B.; Ratner, M. A.; Wasielewski, M. R. *J. Am. Chem. Soc.* **2001**, *123*, 7877–7886.
(88) Laine, P. P.; Loiseau, F.; Campagna, S.; Ciofini, I.; Adamo, C. *Inorg. Chem.* **2006**, *45*, 5538–5551.
(89) Marcus, R. A.; Sutin, N. *Biochim. Biophys. Acta* **1985**, *811*, 265–322.
(90) Demanze, F.; Yassar, A.; Garnier, F. *Macromolecules* **1996**, *29*, 4267–4273.
(91) Zhao, M. T.; Singh, B. P.; Prasad, P. N. *J. Chem. Phys.* **1988**, *89*, 5535–5541.
(92) Kellogg, R. M.; Schaap, A. P.; Wynberg, H. *J. Org. Chem.* **1969**, *34*, 343–346.
(93) Carpita, A.; Rossi, R.; Veracini, C. A. *Tetrahedron* **1985**, *41*, 1919–1929.
(94) Tamao, K.; Kodama, S.; Nakajima, I.; Kumada, M.; Minato, A.; Suzuki, K. *Tetrahedron* **1982**, *38*, 3347–3354.
(95) Kumada, M.; Tamao, K.; Sumitani, K. *Org. Synth.* **1978**, *58*, 127–133.
(96) Hanson, R. W.; Smith, N. G. *Educ. Chem.* **1986**, *23*, 45–46.
(97) Wainer, I. W.; Crabos, M.; Cloix, J. F. *J. Chromatogr.* **1985**, *338*, 417–421.
(98) Feigenbaum, A. *J. Chem. Educ.* **1984**, *61*, 649.
(99) Demas, J. N.; Crosby, G. A. *J. Phys. Chem.* **1971**, *75*, 991–1024.
(100) Sanabria, H.; Miller, J. H., Jr.; Mershin, A.; Luduena, R. F.; Kolomenski, A. A.; Schuessler, H. A.; Nanopoulos, D. V. *Biophys. J.* **2006**, *90*, 4644–4650.
(101) Breitung, E. M.; Vaughan, W. E.; McMahon, R. J. *Rev. Sci. Instrum.* **2000**, *71*, 224–227.
(102) Tjahjono, M.; Davis, T.; Garland, M. *Rev. Sci. Instrum.* **2007**, *78*, 023902/023901–023902/023906.
(103) Vullev, V. I.; Wan, J.; Heinrich, V.; Landsman, P.; Bower, P. E.; Xia, B.; Millare, B.; Jones, G., II. *J. Am. Chem. Soc.* **2006**, *128*, 16062–16072.
(104) Millare, B.; Thomas, M.; Ferreira, A.; Xu, H.; Holesinger, M.; Vullev, V. I. *Langmuir* **2008**, *24*, 13218–13224.

JP810909V